Am J Cancer Res 2023;13(8):3324-3341
www.ajcr.us /ISSN:2156-6976/ajcr0151585

Original Article

Role of LRRN4 in promoting malignant behavior in a p53- and Rb-defective human fallopian tube epithelial cell line

Yu-Hsun Chang[1], Kun-Chi Wu[2], Kai-Hung Wang[3], Dah-Ching Ding[4,5]

[1]Department of Pediatrics, Hualien Tzu Chi Hospital, Buddhist Tzu Chi Medical Foundation, Tzu Chi University, Hualien, Taiwan; [2]Department of Orthopedics, Hualien Tzu Chi Hospital, Buddhist Tzu Chi Medical Foundation, Tzu Chi University, Hualien, Taiwan; [3]Department of Medical Research, Hualien Tzu Chi Hospital, Buddhist Tzu Chi Medical Foundation, Tzu Chi University, Hualien, Taiwan; [4]Department of Obstetrics and Gynecology, Hualien Tzu Chi Hospital, Buddhist Tzu Chi Medical Foundation, Tzu Chi University, Hualien, Taiwan; [5]Institute of Medical Sciences, College of Medicine, Tzu Chi University, Hualien, Taiwan

Received June 4, 2023; Accepted August 1, 2023; Epub August 15, 2023; Published August 30, 2023

Abstract: This study explored the role of leucine-rich repeat neuronal 4 (LRRN4) in ovarian carcinogenesis using the p53- and Rb-defective human fallopian tube epithelial cell line FE25. We evaluated the expression of LRRN4 in FE25 cells with and without LRRN4 knockdown by short hairpin RNA (shRNA) and studied its effects on cell proliferation, cell cycle, migration, invasion, chemotherapeutic sensitivity, apoptosis, and xenograft formation. The results showed that FE25 shRNA-LRRN4 cells exhibited more aggressive malignant behaviors than FE25 cells, including faster proliferation and increased cell distribution in the G2/M phase, Akt pathway activation, cell migration, and cell invasion, as well as decreased sensitivity to chemotherapeutic drugs. FE25 shRNA-LRRN4 cells exhibited reduced levels of apoptosis and decreased expression of cleaved caspase 3, 7, 8, and 9, indicating reduced apoptotic activity. Additionally, FE25 shRNA-LRRN4 cells showed decreased LRRN4 and CK7 expression and increased WT1 expression, suggesting a potential role for LRRN4 in ovarian carcinogenesis. FE25 shRNA-LRRN4 generated a xenograft in mice with increased levels of *WT1* and *TP53* expression compared to their levels in cells. Overall, this study suggests that LRRN4 may play a role in ovarian carcinogenesis by promoting aggressive malignant behavior in FE25 cells through the activation of the Akt pathway. These findings provide insights into the potential molecular mechanisms underlying ovarian cancer and may have implications for the development of new therapeutic targets for this disease.

Keywords: LRRN4, Akt, fallopian tube epithelium, ovarian cancer, shRNA

Introduction

Epithelial ovarian cancer poses a significant global health concern, ranking as the fifth leading cause of cancer-related deaths among women [1, 2]. Among ovarian cancer types, high-grade serous ovarian carcinoma (HGSOC) is particularly fatal, contributing to over 220,000 new cases annually [1]. Tragically, most ovarian cancer cases are diagnosed at an advanced stage, resulting in unfavorable survival rates [1]. The current treatment approach involves debulking surgery and adjuvant chemotherapy, but mortality rates have shown little improvement since 1930, underscoring the critical need for early detection and effective intervention strategies in tackling these cancers [1, 3].

HGSOC is characterized by significant genetic changes, including extensive structural variations, inactivation of the p53 pathway, deficiency in homologous recombination-mediated DNA damage repair (HR DDR) due to mutations in the breast cancer gene 1 (BRCA1), activation of cyclin E1 (CCNE1) and notch receptor 3 (NOTCH3), and inactivation of the retinoblastoma protein (Rb) and neurofibromatosis 1 (NF1) [4, 5]. Tumor protein P53 (TP53) mutations are particularly prevalent, being present in over 96% of HGSOC cases [6]. Subsequent to TP53 mutation, there is an occurrence of deletion or

loss of heterozygosity (LOH) of chromosomes bearing TP53, BRCA1, or BRCA2 genes, leading to homologous recombination defects [6, 7]. Collectively, the gene mutation is vital to the development of HGSOC.

The cell of origin of HGSOC is the fallopian tube epithelium (FTE). To explore the novel gene involved in carcinogenesis, we developed a human FTE cell line (FE25) with p53 and Rb deficiencies [8]. After prolonged in vitro culture, these cells spontaneously transformed into FE25L cells. We compared FE25 and FE25L cells to assess their potential as an ideal cell model for HGSOC [9]. The results revealed that FE25L cells displayed increased cell proliferation, clonogenicity, polyploidy, aneuploidy, cell migration, and invasion, as well as increased resistance to chemotherapy and tumor growth in xenografts. RNA-seq data indicated upregulation of hypoxia, epithelial-mesenchymal transition (EMT), and the NF-κB pathway in FE25L cells. The study suggests that FE25L cells exhibit more aggressive malignant behavior than FE25 cells [9]. Furthermore, our preliminary investigation revealed a notable downregulation of Leucine-rich repeat neuronal protein-4 (LRRN4) in FE25L cells.

LRRN4 is a group of proteins involved in various biological processes, including cytoadhesion, receptor interaction, and intracellular transport [10]. LRRN4 was originally identified as a protein formed during long-term memory and is abundant in the lungs and ovaries [11]. However, studies on the role of LRRN4 in cancer are limited. Previous studies have found that LRRN4 is downregulated in chemo-sensitive ovarian cancer compared to chemo-resistant ovarian cancer and primary mesothelioma [12, 13]. In addition to ovarian cancer and mesothelioma, a recent report investigating the oncogenic role of LRRN4 in colorectal cancer (CRC) indicated that LRRN4 overexpression could enhance colon cancer cell proliferation through the activation of the Akt and ERK signaling pathways [20]. However, whether LRRN4 plays a role in ovarian carcinogenesis requires further investigation.

In light of the above-mentioned evidence and unsolved issues, our study aimed to shed light on the precise expression pattern and carcinogenic function of LRRN4 in FE25 cells. We hypothesized that LRRN4 play a vital role in ovarian carcinogenesis. The findings from this research could offer valuable therapeutic opportunities for addressing HGSOC.

Methods

Public database data analysis of LRRN4

We used an online database to check the *LRRN4* gene-survival relationship. UALCAN (http://ualcan.path.uab.edu) was used to check the gene expression-survival relationship. This database was created using The Cancer Genome Atlas (TCGA) RNA-seq level 3 and clinical data from 31 cancer types. The gene expression levels and related survival in ovarian cancer can be calculated from the online database. We input LRRN4 in the string and then got the result. The Kaplan-Meier plot (LRRN4 high and low expression vs. survival) was shown.

The protein atlas database was used to clarify the protein expression of LRRN4 in the TCGA database. The web address was set as below. Protein atlas database: https://www.proteinatlas.org/ENSG00000125872-LRRN4/pathology/ovarian+cancer.

Pathological validation of LRRN4 in ovarian cancer tissues

Tissue arrays: The tissue arrays used in the study were obtained from US Biomax (Rockville, MD, USA). Specifically, the BC11115 tissue arrays were purchased, which comprised samples of ovarian serous papillary adenocarcinoma, lymph node metastasis, and adjacent normal ovary tissues. These arrays included essential information such as TNM (Tumor, Node, Metastasis) staging and pathology grades for a total of 100 cases with 100 cores.

Immunohistochemistry (IHC) of tissue array: Following the manufacturer's guidelines, immunostaining was conducted using antibodies against LRRN4 (1:200, HPA009431, Sigma-Aldrich). The specimens were then refrigerated at 4°C overnight and subsequently treated with anti-rabbit horse-radish peroxidase-labeled polymer (Dako) for 30 minutes at room temperature. All immunostained slides were co-stained with hematoxylin. For the evaluation of IHC intensity, a semiquantitative score system (immunoreactive score, IRS) was utilized. Staining intensity was graded as negative (1),

Table 1. The primer sequences of the target genes and product size

Name	Forward (5' to 3')	Reverse (5' to 3')	Product size (bp)
LRRN4	TTGGCTCCTCACGGATGCAAAG	AGAGTGGTGCTTTGGTCGGACT	150
PAX8	CAACAGCACCCTGGACGAC	AGGGTGAGTGAGGATCTGCC	113
WT1	GAATGCATGACCTGGAATCA	TCTGCCCTTCTGTCCATTTC	94
TP53	TAACAGTTCCTGCATGGGCG	AGGACAGGCACAAACACGCA	121
GAPDH	CCATCTTCCAGGAGCGAG	GCAGGAGGCATTGCTGAT	233

weak (2), moderate (3), or intense (4). The percentage of stained cells was scored as 0% (0), 1-25% (1), 26-50% (2), 51-75% (3), or 76-100% (4). The sum score, which combined intensity and percentage of staining, was then categorized into low (score 0-4) and high (score 5-7) groups [14]. The final results were presented as a bar chart, with each bar corresponding to different cancer stages. The bar chart depicts the percentage of different IHC intensities observed in various cancer stages. Moreover, the correlation between IHC intensity and cancer stages was calculated to assess any potential associations.

Cell culture

FE25 and FE25L cell lines were obtained from Dr. Chu Tang-Yuan's Lab. Both cells were cultured in MCDB105 and M199 medium (Sigma, St. Louis, MO, USA), respectively, supplemented with 10% fetal bovine serum (FBS, Biological Ind., Kibbutz, Israel), 100 IU/mL penicillin, and 100 μg/mL streptomycin (Sigma) [9]. The cells were grown in a 75-cm^2 culture flask with 12 mL of medium and incubated at 37°C with 5% CO_2. The culture medium was changed every three days, and cell growth was monitored using an inverted microscope. When the cells reached 80% confluence, they were detached and subcultured using 0.05% trypsin (Sigma) and 0.2% EDTA (Biowest, Nuaillé, France).

RNA extraction and cDNA synthesis

In this experiment, the RNeasy Mini kit (QIAGEN, Hilden, Germany) was used to extract RNA from 5×10^5 cells seeded in a 10-cm culture dish. After 24 h of culture, the cells were detached via treatment with 0.05% trypsin and washed twice with 1× phosphate-buffered saline (PBS). RLT lysis buffer (700 μL, Qiagen) was added to lyse the cells, and the solution was triturated several times with a 1-mL micropipette until the cells were completely lysed and the solution became transparent. RNA was extracted from the lysed cells using the RNeasy Mini Kit, according to the manufacturer's instructions. The extracted RNA was quickly stored at -80°C to maintain its stability and prevent degradation. RNA concentration was measured using a spectrophotometer (DU640; Beckman, Pasadena, CA, USA).

The Reverse-iTTM 1st strand synthesis kit (ABgene, Portsmouth, NH, USA) was used for cDNA preparation. First, 1 μg of total RNA was mixed with 1 μL of anchored oligo dT in a total volume of 12 μL, supplemented with DEPC water. The mixture was incubated at 70°C for 5 min and placed on ice. The reaction mixture (8 μL) was then added, which included 4 μL of 5× first-strand synthesis buffer, 2 μL of dNTP mix (5 mM each), 1 μL of 100 mM DTT, and 1 μL of Reverse-iTTM RTase blend. The samples were then incubated at 47°C for 50 min. The reaction was terminated by incubation at 75°C for 10 min. The cDNA was stored at -20°C for later use.

Quantitative polymerase chain reaction (qPCR)

Gene expression was quantified using the ABI Step One Plus system (Applied Biosystems, Waltham, MA, USA) in conjunction with Fast-Start Universal SYBR Green Master (ROX; Roche, Indianapolis, IN, USA) gene expression analysis reagents. GAPDH was used as an internal control to analyze gene expression levels. The primer sequences for the target genes are shown in **Table 1**. Gene expression was quantified by normalizing the data to GAPDH expression and then comparing the relative quantification levels with FE25 levels for fold-change analysis.

Western blotting

Cells were lysed with a lysis buffer composed of 150 mM NaCl, 50 mM Tris-HCl (pH 7.4), and 1%

Table 2. The *LRRN4* shRNA sequence

Gene	Forward (5' to 3')	Reverse (5' to 3')
LRRN4-homo-842	GUCCUUCUGUUCCAGAACUTT	AGUUCUGGAACAGAAGGACTT
LRRN4-homo-967	CACGGAUGCAAAGAGAACUTT	AGUUCUCUUUGCAUCCGUGTT
LRRN4-homo-950	GUCCUAUCGAUCAACCUCUTT	AGAGGUUGAUCGAUAGGACTT

Nonidet P-40 (Sigma), along with a proteinase inhibitor cocktail (Roche, Basel, Switzerland). Electrophoresis was performed using a 10% sodium dodecyl sulfate-polyacrylamide gel, followed by transfer onto a nitrocellulose membrane (Hybond-C Super; GE Healthcare, Little Chalfont, UK). The primary antibodies used were those against LRRN4 (1:1000, HPA00-9431; Sigma-Aldrich, St. Louis, MO, USA), Aktser473, Aktthr308 (1:1000, Sigma), cleaved caspase 3, 7, 8, 9 (1:1000, Sigma) and actin (1:10000; Sigma-Aldrich), with actin serving as the internal control. The membranes were incubated with the primary antibodies overnight at 4°C, followed by incubation with the secondary antibody (horseradish peroxidase-conjugated goat anti-mouse IgG; Jackson ImmunoResearch Laboratories, West Grove, PA, USA) for 1 h at room temperature. Bound antibodies were detected using an enhanced chemiluminescence reagent (ECL; GE, Chicago, IL, USA). To quantify the amount of protein, the data were normalized against actin expression, and the relative quantification was compared to that of the original cells for fold-change analysis.

Downregulation of LRRN4 by short hairpin RNA (shRNA)

The three shRNA were procured from TAQKEY Science Company (Hsinchu, Taiwan), designed for LRRN4 (**Table 2**), and constructed into a lentivirus. We initially tested the multiplicity of infection (MOI) and determined a suitable MOI for transfecting cells. Transfection and antibiotic selection were performed according to the manufacturer's guidelines. To confirm the downregulation of LRRN4 expression (less than 50% relative expression), we performed qPCR following transfection with shRNA or empty vector lentivirus. Upon confirmation of downregulated expression, we performed subsequent characterization experiments. After preliminary experiments, *LRRN4-homo-842* was picked up to do the following experiments.

Cell proliferation following transfection

The XTT assay (Biological Industries, Beit-Haemek, Israel) was used to assess cell proliferation. Cells were seeded at a density of 2×10^3 cells with 100 µL of culture medium per well of a 96-well plate. The optical density of the cells was measured on days 0, 2, 5, and 7. The cells were then incubated with 150 µL of XTT solution at 37°C for 3 h. The optical density was measured at 450 nm using a microplate reader (Model 3550; Bio-Rad, Hercules, CA, USA). Optical density values at each time point were used to generate proliferation curves for the tested cell lines. Cell morphology was also observed under a microscope (NIKON, Tokyo, Japan).

Cell cycle determination

To determine the cell cycle distribution, cells were detached using 0.1% trypsin, resuspended in PBS to reach a concentration of 5×10^6 cells/mL, and washed twice with ice-cold PBS. The cells were incubated in the dark at 0°C with 20 µg/mL propidium iodide (BD Biosciences, San Jose, CA, USA), 0.2 mg/mL RNase A (Invitrogen, Waltham, MA, USA), and 0.1% Triton X-100 (Invitrogen) for 30 min. The percentage distribution of cells in the G0/G1, S, and G2/M phases was analyzed via flow cytometry (BD Biosciences). A total of 10,000 events were processed per specimen, and the FlowJo software (BD Biosciences) was used for analysis.

Anchorage-independent growth (AIG) in soft agar

For the AIG assay, 5×10^5 cells were mixed with 4 mL of 0.35% agarose in a culture medium and then placed on top of 5 mL of 0.7% agarose base in a culture dish. After 14 days of culture, the cells were stained with 0.8 mM crystal violet (Sigma-Aldrich), and the number of colonies was counted. The experiment was performed in triplicate.

Migration and invasion assays

To perform the migration assay, 5×10^4 cells (FE25, FE25-shRNA-NC, and FE25 shRNA-LLRN4) were placed in 200 μL of culture medium in the upper layer of a matrigel-coated transwell Boyden chamber (8 μm pore size; Costar, Corning Inc., Corning, NY, USA) with an 8-μm pore. After 48 h of culture, the cells that migrated to the lower layer were stained with crystal violet (Sigma-Aldrich). The stained cells were counted using an optical microscope. In the invasion assay, 5×10^4 cells were placed in the upper layer of a matrigel-coated transwell chamber and cultured for 48 h. The cells that invaded the lower layer were stained with crystal violet, and the number of invasive cells was counted. Each experiment was performed in triplicate.

Chemosensitivity

The effects of paclitaxel (Formoxol, Yung Shin Pharm. Ind., Co., Ltd., Taichung, Taiwan) and carboplatin (SINPHAR Pharmaceutical Co., Ltd., Yilan, Taiwan), two common chemotherapeutic drugs used to treat ovarian cancer, were investigated in FE25, FE25-shRNA-NC, and FE25 shRNA-LLRN4. We seeded 3×10^3 cells/well in a 96-well plate and treated them with increasing concentrations of the chemotherapeutic drugs for 48 h to determine their half-maximal inhibitory concentration (IC50) values. We measured the cell concentration after chemotherapy by adding XTT solution and recording the optical density value. Apoptosis was evaluated using the terminal deoxynucleotidyl transferase dUTP nick end labeling (TUNEL, Roche, IN, USA) assay according to the manufacturer's recommendations. IC50 values were calculated using a non-linear regression model in GraphPad Prism (version 9.0; GraphPad Software, San Diego, CA, USA).

Xenografting of transfected cells

We conducted a xenograft experiment using immunodeficient NOD-SCID or NOD/Shi-scid/IL-2Rγ^{null} (NOG) mice purchased and raised at the Tzu Chi University Laboratory Animal Center (Hualien, Taiwan). The experimental protocol was approved by the Laboratory Animal Care and Use Committee of Hualien Tzu Chi Hospital. The mice were divided into three groups: untransfected FE25 cells (FE25; n = 2), FE25 cells with non-targeting shRNA (FE25 shRNA-NC; n = 3), and FE25 cells with LRRN4 shRNA (FE25 shRNA-LRRN4; n = 5). We transplanted 1×10^6 cells into the subcutaneous region of the back of each mouse and monitored tumor growth in each group. Tumor volume was calculated using the formula: width^2 × (length/2). When the tumor volume exceeded 500 mm^3 or after six months, the mice were sacrificed, and the tumor was removed and stored in neutral formalin. Mice were euthanasia by CO_2 exposure, followed by decapitation. The percentage of tumorigenesis and xenograft proliferation rates of the test cells among the groups were calculated.

Histopathology and IHC of xenograft tissues

Histological examination of the tumors formed in the xenograft experiments was performed via hematoxylin and eosin (H&E) staining and immunostaining. After removing formalin with xylene and rehydrating, the tissue was treated with an antigen solution (Vector Laboratories, Newark, CA, USA) for unmasking. The intrinsic peroxidase activity was blocked by incubating in 3% hydrogen peroxide in dH_2O. Antibodies against paired box gene 8 (PAX8; 1:1000; Dako, Agilent, Santa Clara, CA, USA) and Wilms tumor 1 (WT1; 1:200; Dako) were used for immunostaining according to the manufacturer's instructions of the respective kits. The slides were co-stained with hematoxylin.

Statistical analysis

For statistical analysis, Student's t-test was used for two groups, and analysis of variance (ANOVA) was used for three or more groups, followed by a post hoc test (Bonferroni test) to determine statistical significance. Statistical significance was set at $P < 0.05$. The results are presented as mean ± standard deviation. GraphPad Prism (version 9.0; GraphPad Software) was used for all calculations. This analysis included proliferation, cell cycle, gene expression, colony number, migration, and cell invasion experiments.

Results

The correlation between the expression of the LRRN4 gene and overall survival in ovarian cancer patients

To examine the correlation between LRRN4 gene expression and overall survival in ovarian

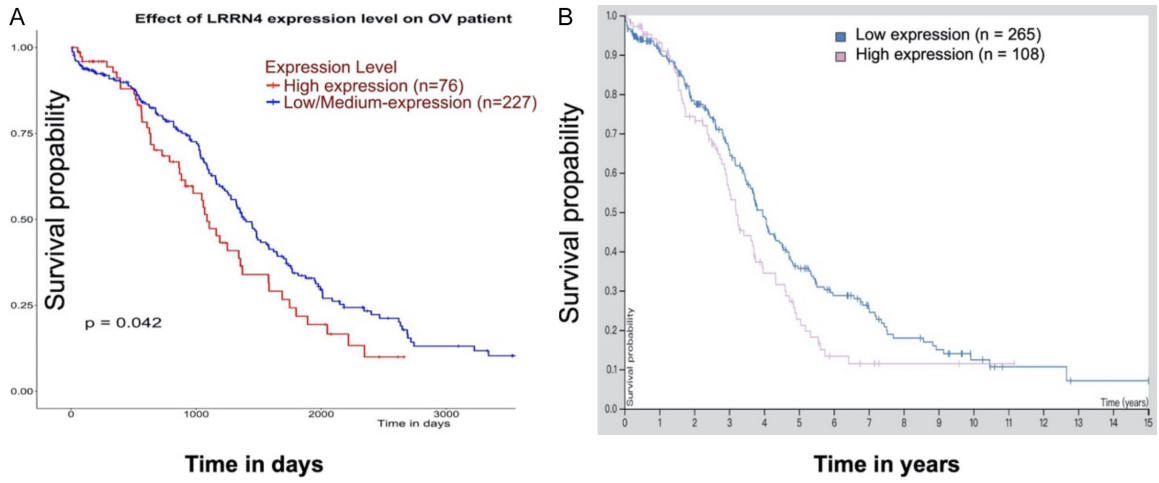

Figure 1. The data presented in this study include RNA and protein expression information obtained from online databases. A. The study explores the correlation between the expression of the LRRN4 gene and overall survival in ovarian cancer patients. The figure was obtained from the online database UALCAN (http://ualcan.path.uab.edu) (High expression, N = 76; low expression, N = 227). B. The study investigates the relationship between the expression of the LRRN4 protein and overall survival in ovarian cancer patients. The figure was derived from the online database Protein Atlas (https://www.proteinatlas.org/ENSG00000125872-RRN4/pathology/ovarian+cancer) (High expression, N = 108; low expression, N = 265).

cancer patients, we utilized an online database, UALCAN (http://ualcan.path.uab.edu). The Kaplan-Meier (K-M) plot based on the data from this database revealed that high expression of the LRRN4 gene (N = 76) was significantly associated with poor survival (P = 0.042) when compared to low expression of this gene (N = 227) (**Figure 1A**). Furthermore, we investigated the relationship between LRRN4 protein expression and overall survival in ovarian cancer patients using the online database Protein Atlas (https://www.proteinatlas.org/ENSG00000125872-LRRN4/pathology/ovarian+cancer). The K-M plot analysis, with data from 108 patients with high LRRN4 protein expression and 265 patients with low expression, did not show any significant association between LRRN4 protein levels and overall survival (**Figure 1B**). In summary, the above studies present conflicting results, creating controversy regarding the role of LRRN4 in ovarian cancer patients.

Normal and malignant ovarian tissues expressed LRRN4 proteins which did not correlate with stage

To determine the expression of LRRN4 in malignant ovarian tissue, a tissue array including both normal and malignant ovarian tissues, was utilized. The tissue array, comprising 100 samples (**Figure 2A**), was stained with LRRN4 (**Figure 2B**). Subsequently, the IRS score of LRRN4 was evaluated across different stages of ovarian cancer (**Figure 2C**). The investigation into the correlation between LRRN4 expression and the stage of ovarian cancer resulted in an R2 value of 0.0243 (**Figure 2D**). Additionally, the distribution of different degrees of staining was analyzed in relation to various stages of ovarian cancer (**Figure 2E**). Overall, the study did not find any association between the intensity of LRRN4 staining and the stage of ovarian cancer.

Transfection of shRNA decreased LRRN4 expression, increases proliferation, and alters cell cycle distribution

Following shRNA transfection into FE25 cells, LRRN4 expression, cell proliferation, cell cycle distribution, and signaling pathway component expression were investigated. The transfection of shRNA-LRRN4 led to a decrease in both the gene and protein expression of LRRN4 compared to those in FE25 cells (**Figure 3A** and **3B**); however, the cell morphology remained unchanged after shRNA transfection (**Figure 3C**). The proliferation rate was increased in FE25 shRNA-LRRN4 cell compared to that in FE25 shRNA-NC and FE25 cells, as determined by the XTT assay (**Figure 4A**). Cell cycle distribu-

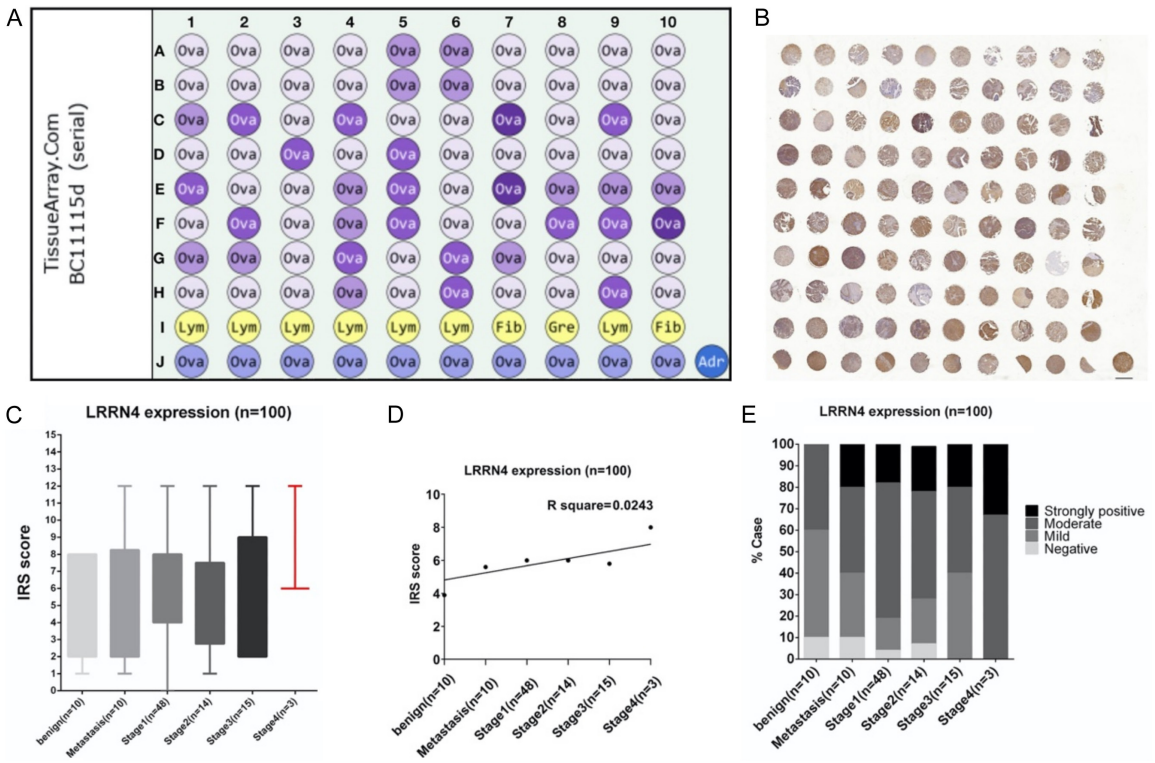

Figure 2. The immunohistochemical analysis of tissue array comprising normal and malignant ovarian tissues. A. Composition of the tissue array. B. Immunohistochemistry was performed on the tissue array to examine ovarian cancer samples (N = 100). C. The immunoreactive score (IRS) of LRRN4 was assessed across different stages of ovarian cancer. D. The correlation between LRRN4 expression and the stage of ovarian cancer was investigated. E. The distribution of different degrees of staining was analyzed with various stages of ovarian cancer. Abbreviations: Fib: Fibrofatty tissue, Gre: Greater omentum, Lym: Lymph node, Ova: Ovary. Color meaning: light purple circle - Malignant tumor (stage I), second deep purple circle - Malignant tumor (stage II), third deep purple circle - Malignant tumor (stage III), deep purple circle - Malignant tumor (stage IV), yellow circle - Metastasis, Line J - normal ovarian tissue.

tion analysis revealed an increased percentage of cells in the G2/M phase in FE25 shRNA-LRRN4 cells compared to that in FE25 and FE25 shRNA-NC cells ($P < 0.001$, **Figure 4B-F**). Among the signaling pathway components evaluated, increased expression was observed in Akt (**Figure 5**), while no significant change was seen for β-catenin or TGF-β (data not shown).

Knockdown of LRRN4 produced chemoresistance to paclitaxel and carboplatin

The IC50 values of paclitaxel and carboplatin were evaluated in the three cell lines to test the chemosensitivity. Following treatment, the IC50 value of paclitaxel in FE25, FE25 shRNA-NC, and FE25 shRNA-LRRN4 cells was 3.57, 2.41, and 2.13 nM, respectively (**Figure 6A-C**). The IC50 value of carboplatin was 26.43, 11.38, and 42.82 μM, respectively (**Figure 6D-F**). The findings demonstrated that down-regulation of LRRN4 led to enhanced resistance against carboplatin, but it did not affect resistance to paclitaxel.

Knockdown of LRRN4 produced chemoresistance to carboplatin-induced apoptosis

The TUNEL assay was then used to assess apoptosis following carboplatin and paclitaxel treatment. The results showed an increase in apoptosis in FE25 and FE25 shRNA-NC cells (**Figure 7A**, **7B**), but no significant change in FE25 shRNA-LRRN4 cells after carboplatin treatment (**Figure 7C**). An increase in apoptosis was observed in all cell types after paclitaxel treatment (**Figure 8**).

The apoptotic signaling pathway was evaluated further by examining cleaved caspases 3, 7, 8, and 9 using Western blot. Following paclitaxel

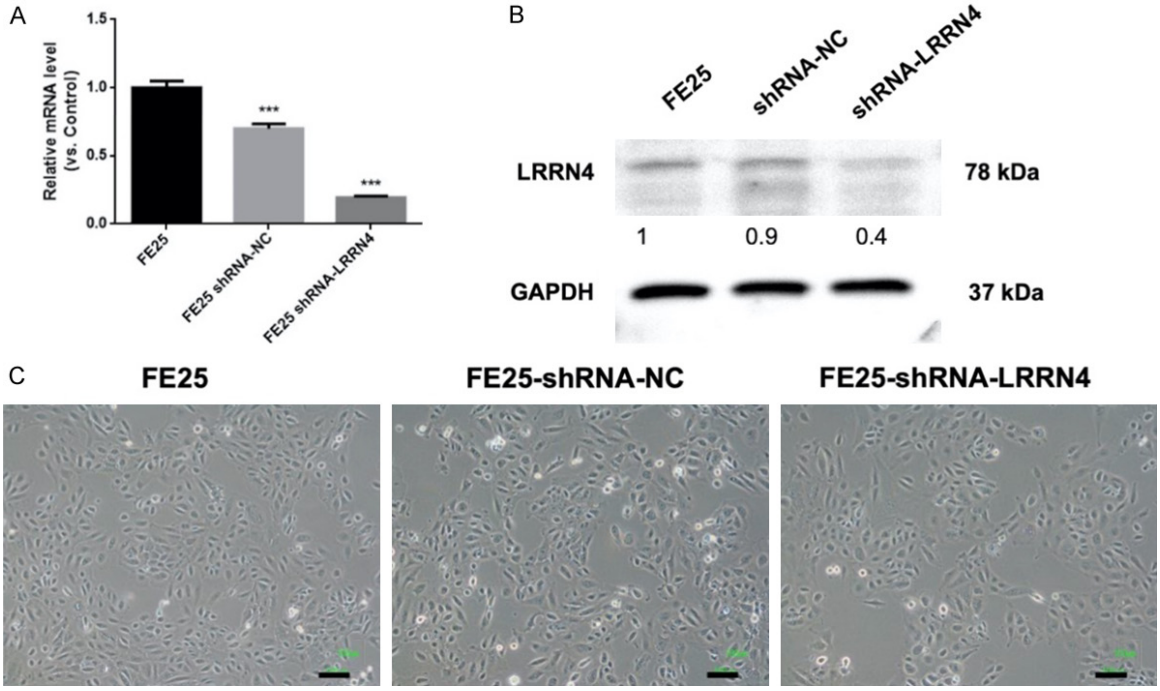

Figure 3. Knockdown of *LRRN4* expression in FE25 cells using shRNA. The knockdown was confirmed through (A) quantitative polymerase chain reaction (N = 3) and (B) western blot analysis. The image was representative of N = 3. (C) The cell morphology was observed after knockdown experiments. Scale bar = 100 μm. shRNA: short hairpin RNA. NC: control shRNA. ***P < 0.001 compared to untransfected FE25.

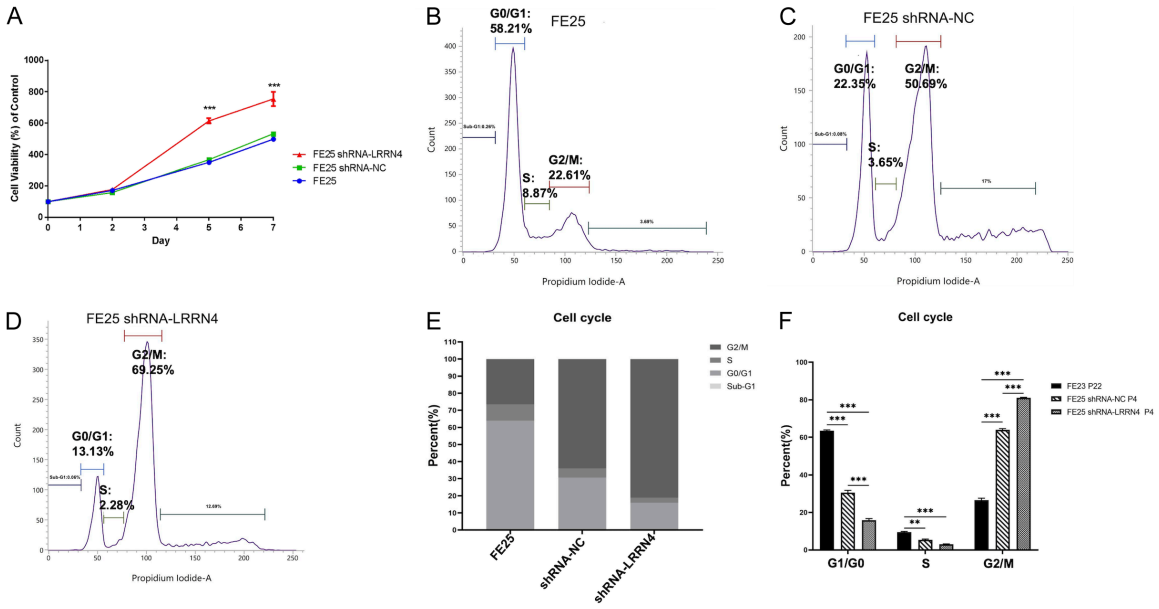

Figure 4. The effect of LRRN4 knockdown on proliferation and cell cycling of FE25 cells. (A) The proliferation curve of FE25 cells with or without LRRN4 knockdown. Flow cytometry was used to analyze the cell cycle of (B) FE25 cells, (C) FE25 cells with non-targeting shRNA (FE25 shRNA-NC), and (D) FE25 cells with LRRN4 shRNA (FE25 shRNA-LRRN4). The image was representative of N = 3. The percentage of cells in various cell cycle phases was then (E) calculated for each cell line and (F) compared between cell lines. The experiments were performed in triplicate. ***P < 0.001.

and carboplatin treatment, the expression levels of cleaved caspases 3, 7, 8, and 9 were lower in FE25 shRNA-LRRN4 cells than in FE25 and FE25 shRNA-NC cells (**Figure 9**).

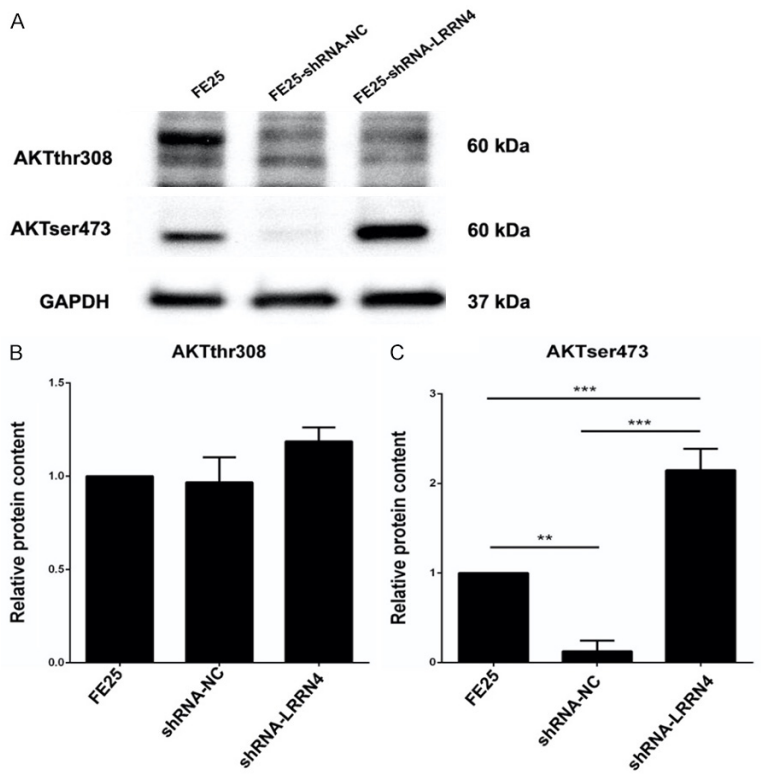

Figure 5. The Akt signaling pathway in FE25 cells with and without knockdown of LRRN4. A. Western blot analysis was performed to measure the expression of Aktser473 and Aktthr308 among FE25, FE25 shRNA-NC, and FE25 shRNA-LRRN4. The image was representative of N = 3. B. Aktser473. C. Aktthr308. **P < 0.01, ***P < 0.001. After the knockdown of LRRN4, Akt significantly increased expression (P < 0.001). After transfection of shRNA-NC, Akt significantly decreased expression (P < 0.01).

Knockdown of LRRN4 increased cell migration and invasion

Transwell migration and invasion assays were employed to investigate the impact of LRRN4 knockdown on cell migration and invasion. FE25 shRNA-LRRN4 cells exhibited significantly higher cell migration (P < 0.05, **Figure 10A**, **10B**) than FE25 and FE25 shRNA-NC. Moreover, cell invasion was nearly doubled in FE25 shRNA-LRRN4 cells (P < 0.001, **Figure 10C**, **10D**) when compared to both FE25 and FE25 shRNA-NC. These findings strongly suggest that LRRN4 knockdown enhances the migration and invasion capabilities of FE25 cells.

Knockdown of LRRN4 did not affect AIG

The AIG activity is commonly employed to assess the clonogenicity of cancer cells. However, in this study, clonogenicity remained unaffected, as indicated by the AIG assay, which showed no difference in colony formation among FE25, FE25 shRNA-NC, and FE25 shRNA-LRRN4 cells (**Figure 11**). These results suggest that LRRN4 knockdown did not lead to an increase in stemness of FE25 cells.

Knockdown of LRRN4 decreased LRRN4 and CK7 expression and increased WT1 expression in FE25 cells

IHC was performed to assess the protein expression of LRRN4, CK7, and WT1 in the FE25 and transfected cells. The findings revealed that FE25 shRNA-LRRN4 cells exhibited decreased expression of both LRRN4 and CK7 (P < 0.001) but showed an elevated expression of WT1 (P < 0.001) compared to FE25 cells (**Figure 12**). These results strongly suggest that LRRN4 knockdown resulted in an upregulation of the oncoprotein WT1.

The FE25 shRNA-LRRN4 xenograft increased TP53 and WT1 expression

To assess the in vivo tumorigenic potential of the three cell lines, xenografts were implanted into immunodeficient mice. After 218 days, a xenograft was successfully generated from the FE25 shRNA-LRRN4 cell line (**Figure 13A**). The resulting tumor displayed a smooth surface and measured 0.5 cm in diameter (**Figure 13B**). In contrast, no xenografts were observed from the FE25 or FE25 shRNA-NC cell lines. The tumorigenic efficiency of FE25 shRNA-LRRN4 was determined to be 20%, while the other two cell lines did not exhibit any tumorigenesis (**Figure 13C**).

In the FE25 shRNA-LRRN4 xenograft, we conducted examinations on gene and protein expression, as well as histology. Gene expression analysis revealed an upregulation of *PAX8*,

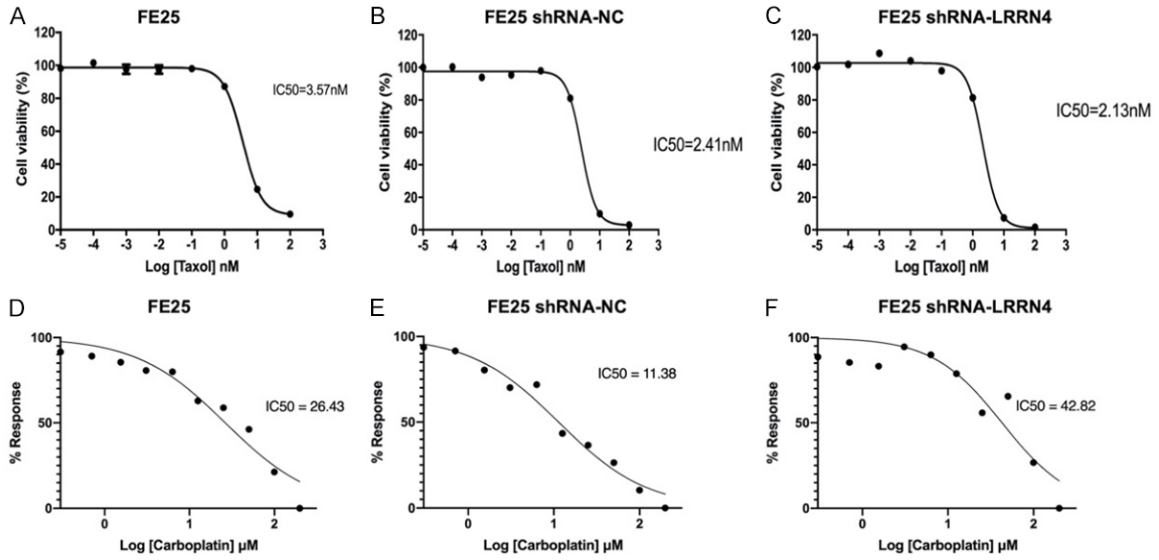

Figure 6. Chemosensitivity analysis of different cell lines treated with carboplatin and paclitaxel. The half maximal inhibitory concentration (IC50) curve of paclitaxel in (A) FE25, (B) FE25 shRNA-NC, and (C) FE25 shRNA-LRRN4 cells. The IC50 curve of carboplatin in (D) FE25, (E) FE25 shRNA-NC, and (F) FE25 shRNA-LRRN4 cells. The image was representative of N = 3.

TP53, and *WT1* in the xenograft compared to the in vitro cells (**Figure 14A**). Histological examination exhibited a sheet of epithelioid tumor cells displaying vesicular nuclei, single prominent nucleoli, an increased nuclear/cytoplasm ratio, and mitosis (**Figure 14B**). IHC further confirmed the expression of WT1 and PAX8 in the tumor (**Figure 14C**, **14D**).

These findings suggest that LRRN4 knockdown may contribute to enhanced tumorigenic potential and altered gene and protein expression in ovarian cancer cells.

Discussion

The study's results revealed that the downregulation of LRRN4 in FE25 cells led to heightened aggressive behaviors, including increases in proliferation, mitosis, migration, invasion, chemoresistance, and a reduction in apoptosis. Moreover, the increased proliferation of FE25 shRNA-LRRN4 cells was associated with elevated phosphorylation of Akt. Additionally, the downregulation of LRRN4 in FE25 cells resulted in the generation of a xenograft with higher expression of WT1 and TP53 compared to control cells. These findings suggest that LRRN4 plays a crucial role in regulating various oncogenic processes and may have implications for ovarian cancer progression and treatment response.

Previous studies indicate that the role of LRRN4 in oncogenesis is not yet fully understood. Some studies have reported LRRN4 downregulation in certain types of cancers, such as primary mesothelioma and chemo-sensitive ovarian cancer [12, 13]. However, a recent study reported upregulation of LRRN4 in HGSOC [15]. This study also suggested that LRRN4 interacts with other genes and pathways to promote oncogenesis; an interaction between LRRN4 and TOP2A in HGSOC was observed, which may be related to the TGF-β/Smad pathway [15]. In the present study, the downregulation of LRRN4 in FE25 cells led to increased malignant behaviors and Akt signaling was found to be involved in this event. The roles of LRRN4 in ovarian pre-cancer and cancer may also differ and require further investigation. Overall, the available evidence suggests that LRRN4 plays a complex role in oncogenesis, and further studies are needed to understand its function in different types of cancer fully.

A recent report on the oncogenic role of LRRN4 in colorectal cancer (CRC) suggested that LRRN4 overexpression can increase colon cancer cell proliferation via the Akt and ERK signaling pathways [16]. This finding is consistent with our study, which identified Akt signaling pathway involvement in promoting proliferation

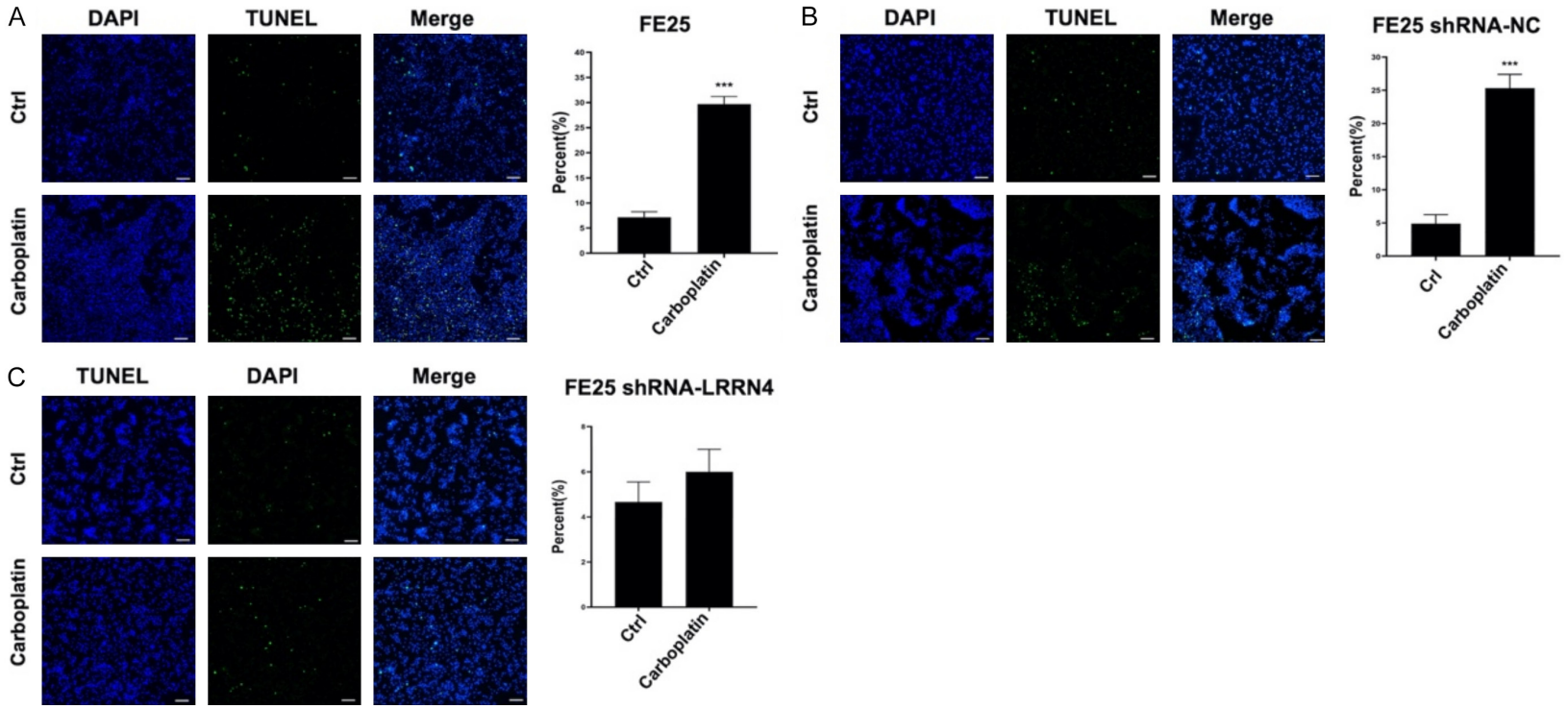

Figure 7. Terminal deoxynucleotidyl transferase dUTP nick end labeling (TUNEL) assay before and after treatment with carboplatin (half maximal inhibitory concentration) for 72 h. The graphs show the TUNEL assay results for (A) FE25, (B) FE25 shRNA-NC, and (C) FE25 shRNA-LRRN4 cells. All experiments were repeated three times, and the data are expressed as mean ± SEM. **P < 0.01, ***P < 0.001 compared with untreated cells. After treatment with carboplatin, $TUNEL^+$ cells were increased.

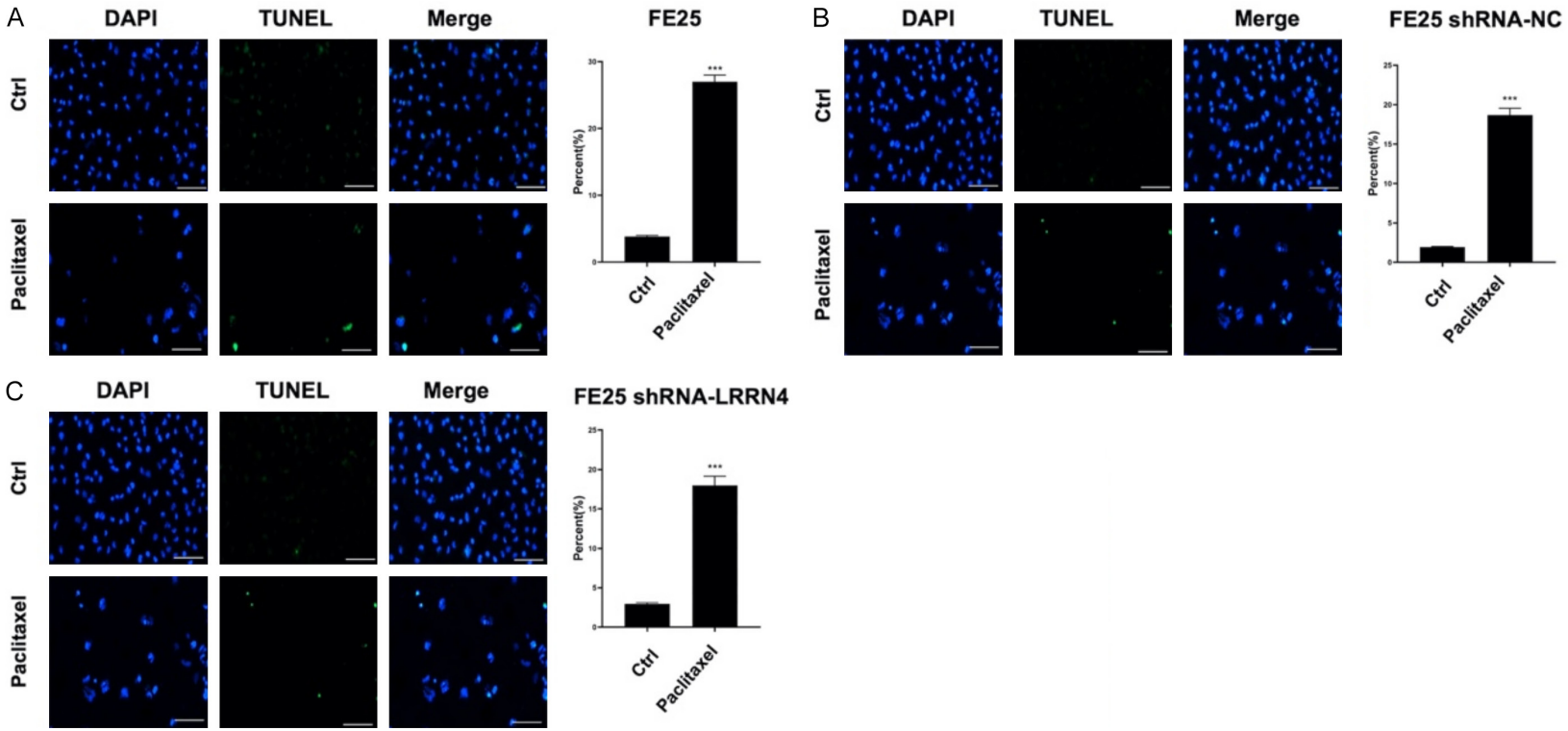

Figure 8. Terminal deoxynucleotidyl transferase dUTP nick end labeling (TUNEL) assay before and after treatment with paclitaxel (half maximal inhibitory concentration) for 72 h. The graphs show the TUNEL assay results for (A) FE25, (B) FE25 shRNA-NC, and (C) FE25 shRNA-LRRN4 cells. All experiments were repeated three times, and the data are expressed as mean ± SEM. ***P < 0.001 compared with untreated cells. After treatment with paclitaxel, $TUNEL^{+}$ cells were increased.

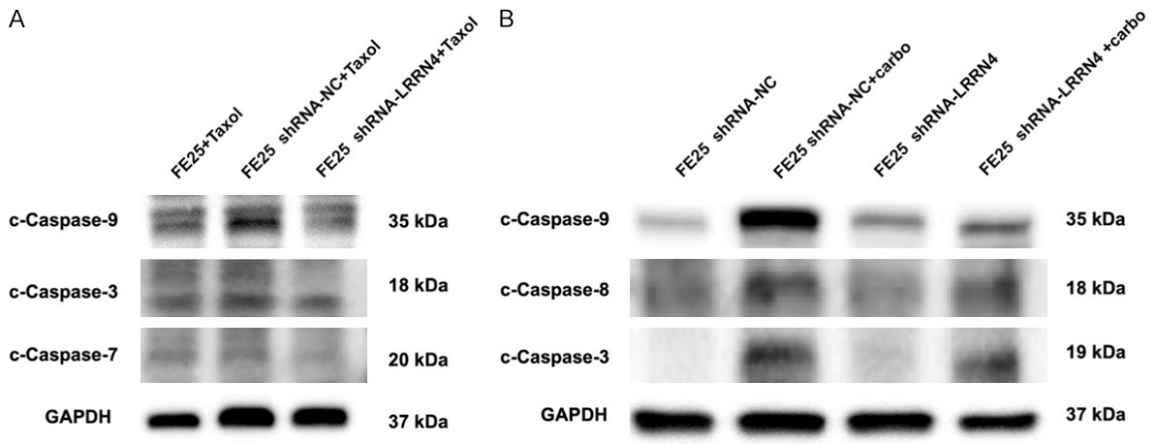

Figure 9. Western blot analysis of apoptosis-associated protein expression after treatment with chemotherapy drugs. Cleaved (c)-caspases 3, 7, 8, and 9 were analyzed in response to treatment with (A) paclitaxel (taxol) and (B) carboplatin (carbo) in FE25, FE25 shRNA-NC, and FE25 shRNA-LRRN4 cells. After treatment with carboplatin, the expressions of cleaved caspase 3, 8, 9 were increased.

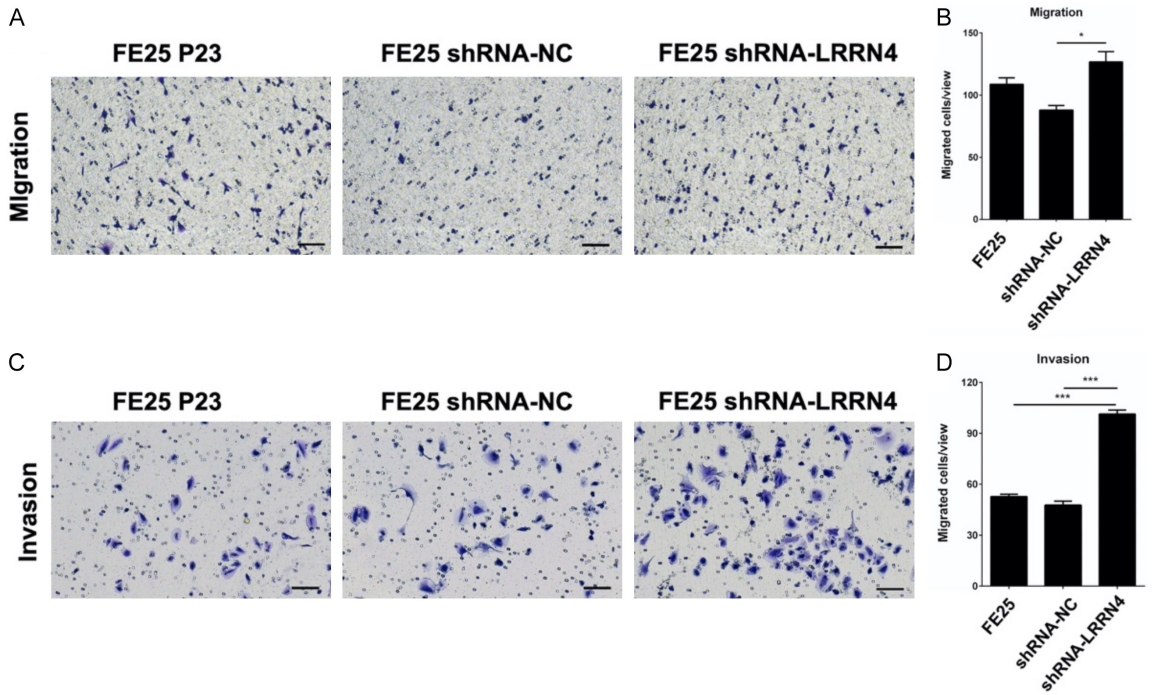

Figure 10. Migration and invasion assay of FE25 cells with or without *LRRN4* knockdown. A. Transwell migration assay for 48 hours. Gross picture of migration cells stained with crystal violet. B. Quantification of migrated cells. *P < 0.05 when compared to FE25. C. Transwell invasion assay for 48 h. Gross picture of invaded cells stained with crystal violet. D. Quantification of invaded cells. *P < 0.05 when compared to FE25. *P < 0.05, ***P < 0.001. All experiments were repeated in triplicate. The image was representative of N = 3.

in FE25 cells with downregulated LRRN4 expression. A study on CRC also reported a correlation between increased LRRN4 expression and poor prognosis and survival, suggesting that LRRN4 may serve as a potential biomarker for CRC [16]. Contrary to this, another study showed that LRRN4 expression was lower in CRC tumors than in normal tissues [17]. This discrepancy may be due to differences in sample size, patient population, or experimental methods used in the studies. Similarly, a study on gastric cancer identified LRRN1 as a prog-

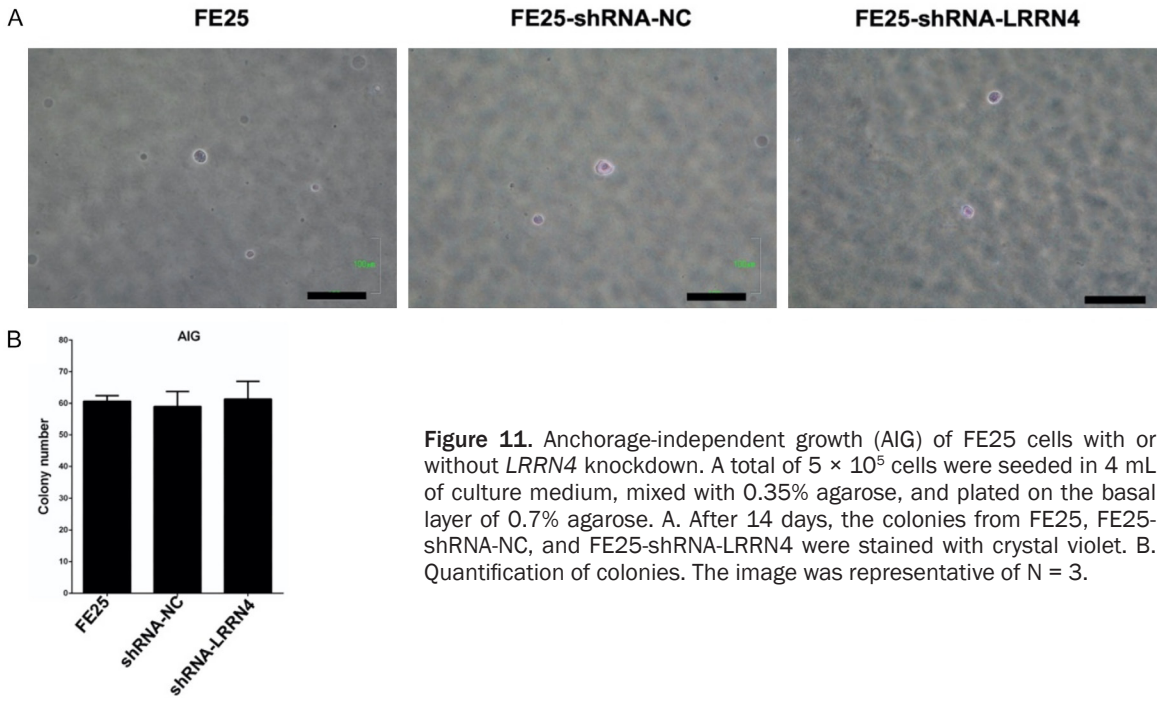

Figure 11. Anchorage-independent growth (AIG) of FE25 cells with or without *LRRN4* knockdown. A total of 5 × 10^5 cells were seeded in 4 mL of culture medium, mixed with 0.35% agarose, and plated on the basal layer of 0.7% agarose. A. After 14 days, the colonies from FE25, FE25-shRNA-NC, and FE25-shRNA-LRRN4 were stained with crystal violet. B. Quantification of colonies. The image was representative of N = 3.

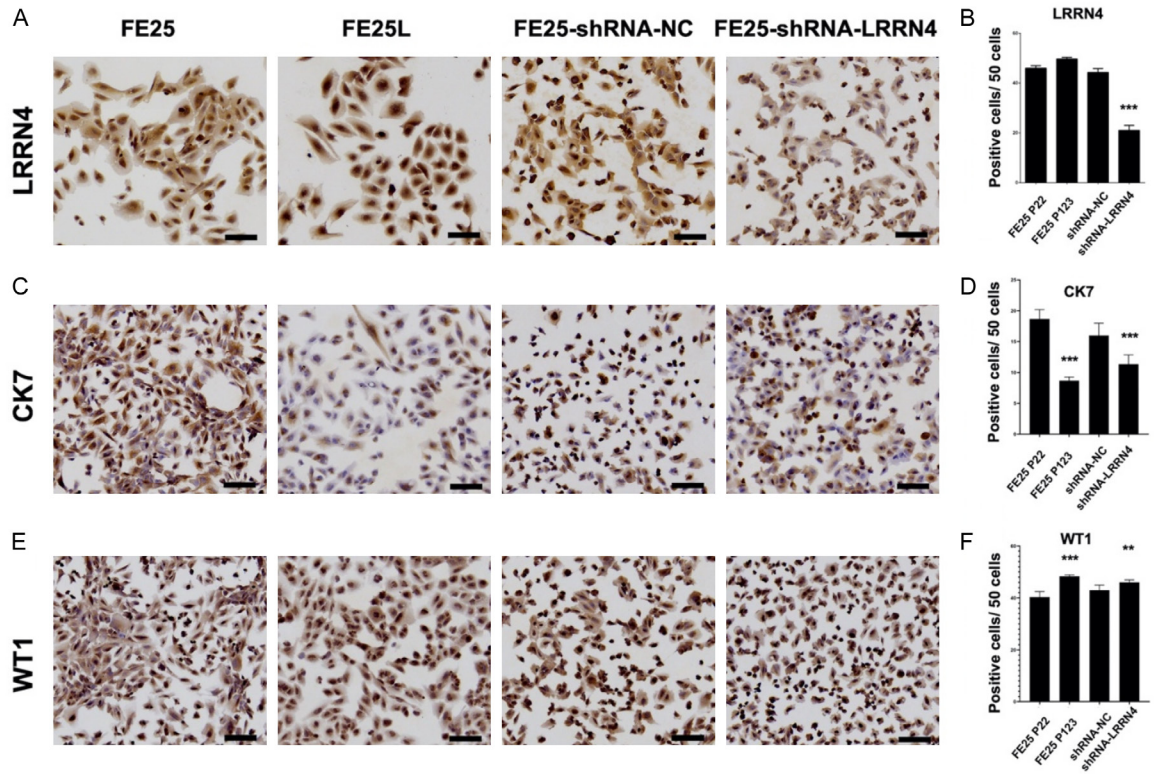

Figure 12. Immunohistochemistry (IHC) of LRRN4, CK7, and WT1 with or without *LRRN4* knockdown. Passage 22 and 123 of FE25 (FE25 P22 and FE25 P123), FE25-shRNA-NC, and FE25-shRNA-LRRN4 were included. A. IHC of LRRN4. B. Quantification of IHC intensity of LRRN4. C. IHC of CK7. D. Quantification of IHC intensity of CK7. E. IHC of WT1. F. Quantification of IHC intensity of WT1. **P < 0.01, ***P < 0.001. Scale bar = 100 μm. The image was representative of N = 3.

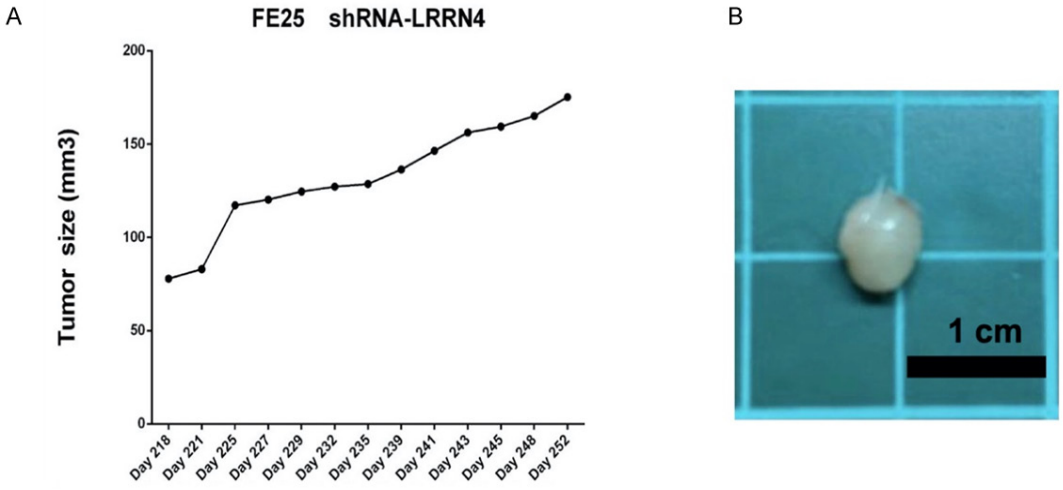

C

Cell line	Number	Tumorigenesis	Tumor size
FE25 P25	2	0	
FE25 shRNA-NC	3	0	
FE25 shRNA-LRRN4	5	1	175mm^3

Figure 13. The proliferation curve and the gross picture of xenograft of FE25 shRNA-LRRN4. A. Proliferation curve of the tumor. B. Gross picture of the tumor. C. The number of xenografts generated from FE25, FE25 shRNA-NC, and FE25 shRNA-LRRN4 cell lines. Scale bar = 1 cm.

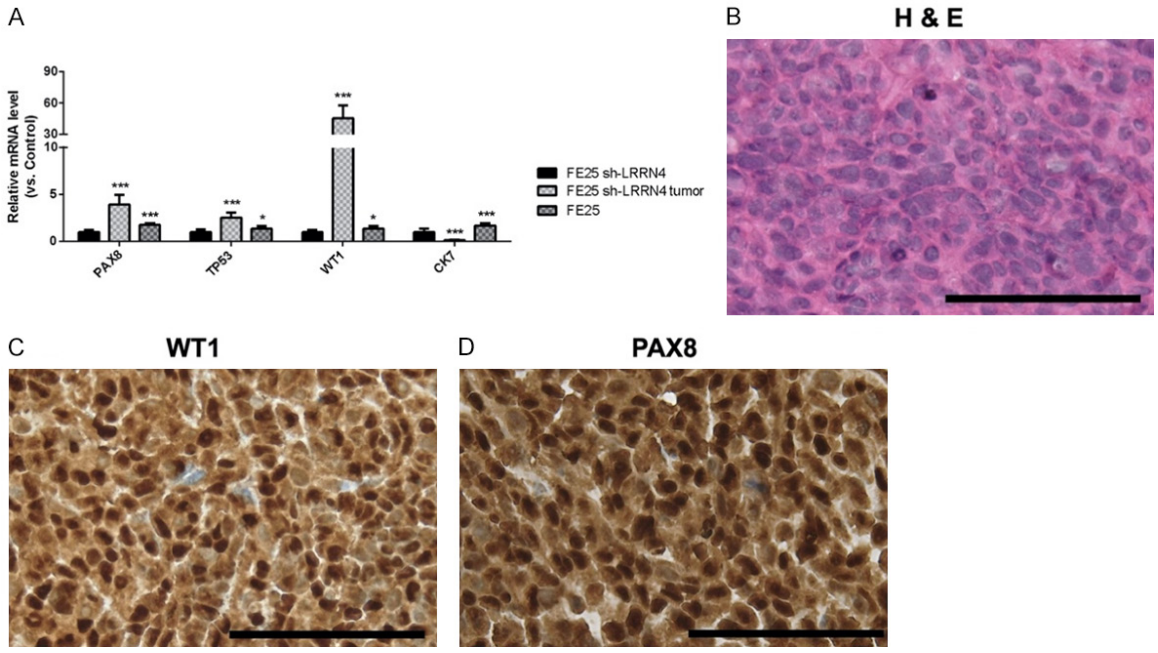

Figure 14. Gene expression, histology, and immunohistochemistry (IHC) of LRRN4-knockdown FE25 cell-generated xenografted tumor (N = 1). (A) The quantitative polymerase chain reaction of gene expression of the tumor and FE25 shRNA-LRRN4 and FE25 cells (N = 3). (B) Hematoxylin and eosin stain (H&E) staining of the tumor. A sheet of epithelioid tumor cells with vesicular nuclei, single prominent nucleoli, increased nuclear/cytoplasm ratio, and mitosis are seen. IHC of (C) WT1 and (D) PAX8. Scale bar = 100 μm.

nostic factor of poor survival via regulation of the Fas/FasL signaling pathway [17]. This finding differs from that regarding LRRN4 in HGSOC in this study, which identified a potential oncogenic role for LRRN4 via the Akt signaling pathway. These differences may be attributed to the differences in cancer types and the underlying mechanisms involved in the pathogenesis of different types of cancer. Overall, the available evidence suggests that LRRN4 may have different roles in different types of cancer, and further studies are needed to understand its functions fully.

LRRN4 shows downregulation in certain types of cancers, including malignant mesothelioma. Malignant mesothelioma is among the most lethal and challenging cancers to treat globally [18]. The median survival rate from diagnosis is approximately 9 months, and 94% of patients do not survive beyond 3 years after diagnosis [18]. LRRN4 is presented in the primary mesothelial cells (can be used as a mesothelial cell marker) and lost or downregulation in mesothelioma cell lines [12]. Another study showed downregulation of LRRN4 in cardiomyocytes may be associated with dilated cardiomyopathy [19]. Above all, the role of LRRN4 in other tumors needs to be studied and needs further exploration.

Our results showed a discrepancy between LRRN4 and ovarian cancer survival. Higher *LRRN4* gene expression was associated with a lower survival rate than low expression of this gene (**Figure 1**). However, regarding protein expression, neither the online database nor our tissue array found its expression associated with ovarian cancer survival or stages (**Figure 2**). Therefore, the prognostic value of LRRN4 in ovarian cancer was uncertain and needed extensive exploration. The biological function of LRRN4 might impact cell adhesion, signaling pathways, or interactions with the tumor microenvironment [16].

It is clear from the available evidence that LRRN4 is associated with several signaling pathways involved in oncogenesis, including the MAPK, Ras, Wnt/β-catenin, and PI3K pathways [20]. The specific role of LRRN4 in each pathway may vary depending on the cancer type and specific signaling context. For example, LRRN4 activates the TGF-β/Smad pathway in HGSOC [15], whereas it activates the Ras/MAPK pathway in CRC [16]. The overexpression of LRRN4 was also found to upregulate the expression of Akt and ERK, which are downstream targets of multiple signaling pathways [16, 21]. In our study, we explored several signaling pathways, including the RAS/MAPK, TGF-β/Smad, and Wnt/β-catenin pathways, and found that Akt was activated by downregulating LRRN4 expression in FE25 cells. This result is similar to that of a previous study on CRC that identified the Ras/MAPK pathway as a key target of LRRN4 [16]. These differences suggest that the specific role of LRRN4 in oncogenesis may be influenced by the type of cancer and specific signaling context [22, 23]. Overall, the available evidence suggests that LRRN4 plays a complex role in oncogenesis by interacting with multiple signaling pathways involved in different aspects of cancer development and progression. Further studies are needed to fully elucidate the specific role of LRRN4 in each pathway and its contribution to the pathogenesis of different cancer types.

Different chemotherapy methods have different therapeutic effects. Neo-adjuvant chemotherapy (NACT) has been implemented mostly in treating advanced ovarian cancer disease [24]. NACT usually performs for 3-4 cycles of chemotherapy and then takes interval debulking surgery (IDS). The progression-free survival and overall survival are not different between patients with primary debulking surgery followed by adjuvant chemotherapy and patients with NACT followed by interval debulking surgery [24]. NACT has been found to enhance immune infiltration and increase programmed death ligand-1 (PD-L1) expression in HGSOC [25]. This treatment also triggers local immune activation, potentially boosting the immunogenicity of these tumors. However, the effectiveness of combining NACT with bevacizumab, Poly (ADP-ribose) polymerase (PARP) inhibitors, or immunotherapy is yet to be assessed and requires further evaluation [26].

Conclusions

Decreased LRRN4 expression in FE25 cells led to more aggressive malignant behavior. The experiments conducted in this study showed that the downregulation of LRRN4 promoted cell proliferation, mitosis, migration, and inva-

sion while inhibiting apoptosis. This was primarily due to the activation of the Akt signaling pathway. Furthermore, the downregulation of LRRN4 can generate xenografts and increase the expression of *WT1* and *TP53*. These findings suggest that LRRN4 plays an oncogenic role in HGSOC. Therefore, LRRN4 may be a promising preventative and therapeutic target for this type of cancer. Overall, this study provides important insights into the role of LRRN4 in HGSOC and highlights the potential for LRRN4 as a therapeutic target.

Acknowledgements

The authors would like to acknowledge funding support from the Ministry of Science and Technology of Taiwan (MOST 110-2314-303-007). This study was also funded by the Buddhist Tzu Chi Medical Foundation (TCRD-111-80, TCMF-EP 111-01, TCRD 111-057, and TCMF-CP 111-05).

Disclosure of conflict of interest

None.

Abbreviations

ANOVA, Analysis of Variance; BRCA1/2, Breast cancer gene 1/2; CCNE1, Cyclin E1; CK7, Cytokeratin 7; CRC, Colorectal cancer; FE25L, High passage FE25; FTEC, Fallopian tube epithelial cell; H&E, Hematoxylin and eosin; HGSOC, High-grade serous ovarian carcinoma; HR DDR, Homologous recombination-mediated DNA damage repair; IC50, Half-maximal inhibitory concentration; IHC, Immunohistochemistry; LOH, Loss of heterozygosity; LRRN4, Leucine-rich repeat neuronal protein-4; NF1, Neurofibromatosis 1; NOG, NOD/Shi-scid/IL-2Rγ^{null}; MOI, Multiplicity of infection; NOTCH3, Notch receptor 3; PAX8, Paired box gene 8; PBS, Phosphate buffered saline; qPCR, Quantitative polymerase chain reaction; shRNA, Short hairpin RNA; Rb, Retinoblastoma protein; TP53, Tumor protein P53; TUNEL, Terminal deoxynucleotidyl transferase dUTP nick end labeling; WT1, Wilms tumor 1.

Address correspondence to: Dr. Dah-Ching Ding, Department of Obstetrics and Gynecology, Hualien Tzu Chi Hospital, Buddhist Tzu Chi Medical Foundation, Tzu Chi University, Hualien, Taiwan. Tel: +886-3-856-1825; Fax: +886-3-857-7161; E-mail: dah-1003@yahoo.com.tw

References

[1] Reid BM, Permuth JB and Sellers TA. Epidemiology of ovarian cancer: a review. Cancer Biol Med 2017; 14: 9-32.

[2] Zhang Y, Luo G, Li M, Guo P, Xiao Y, Ji H and Hao Y. Global patterns and trends in ovarian cancer incidence: age, period and birth cohort analysis. BMC Cancer 2019; 19: 984.

[3] Morrison J, Haldar K, Kehoe S and Lawrie TA. Chemotherapy versus surgery for initial treatment in advanced ovarian epithelial cancer. Cochrane Database Syst Rev 2012; 2012: CD005343.

[4] Kurman RJ and Shih IeM. The origin and pathogenesis of epithelial ovarian cancer: a proposed unifying theory. Am J Surg Pathol 2010; 34: 433-443.

[5] Kurman RJ and Shih IeM. The dualistic model of ovarian carcinogenesis: revisited, revised, and expanded. Am J Pathol 2016; 186: 733-747.

[6] Zhang Y, Cao L, Nguyen D and Lu H. TP53 mutations in epithelial ovarian cancer. Transl Cancer Res 2016; 5: 650-63.

[7] Hoogstraat M, de Pagter MS, Cirkel GA, van Roosmalen MJ, Harkins TT, Duran K, Kreeftmeijer J, Renkens I, Witteveen PO, Lee CC, Nijman IJ, Guy T, van 't Slot R, Jonges TN, Lolkema MP, Koudijs MJ, Zweemer RP, Voest EE, Cuppen E and Kloosterman WP. Genomic and transcriptomic plasticity in treatment-naive ovarian cancer. Genome Res 2014; 24: 200-211.

[8] Huang HS, Chu SC, Hsu CF, Chen PC, Ding DC, Chang MY and Chu TY. Mutagenic, surviving and tumorigenic effects of follicular fluid in the context of p53 loss: initiation of fimbria carcinogenesis. Carcinogenesis 2015; 36: 1419-1428.

[9] Chang YH, Chu TY and Ding DC. Spontaneous transformation of a p53 and Rb-defective human Fallopian tube epithelial cell line after long passage with features of high-grade serous carcinoma. Int J Mol Sci 2022; 23: 13843.

[10] Ng AC, Eisenberg JM, Heath RJ, Huett A, Robinson CM, Nau GJ and Xavier RJ. Human leucine-rich repeat proteins: a genome-wide bioinformatic categorization and functional analysis in innate immunity. Proc Natl Acad Sci U S A 2011; 108 Suppl 1: 4631-4638.

[11] Bando T, Sekine K, Kobayashi S, Watabe AM, Rump A, Tanaka M, Suda Y, Kato S, Morikawa Y, Manabe T and Miyajima A. Neuronal leucine-rich repeat protein 4 functions in hippocampus-dependent long-lasting memory. Mol Cell Biol 2005; 25: 4166-4175.

[12] Kanamori-Katayama M, Kaiho A, Ishizu Y, Okamura-Oho Y, Hino O, Abe M, Kishimoto T, Sekihara H, Nakamura Y, Suzuki H, Forrest AR and

Hayashizaki Y. LRRN4 and UPK3B are markers of primary mesothelial cells. PLoS One 2011; 6: e25391.
[13] Choi CH, Choi JJ, Park YA, Lee YY, Song SY, Sung CO, Song T, Kim MK, Kim TJ, Lee JW, Kim HJ, Bae DS and Kim BG. Identification of differentially expressed genes according to chemosensitivity in advanced ovarian serous adenocarcinomas: expression of GRIA2 predicts better survival. Br J Cancer 2012; 107: 91-99.
[14] Chen Y, Lin G, Guo ZQ, Zhou ZF, He ZY and Ye YB. Effects of MICA expression on the prognosis of advanced non-small cell lung cancer and the efficacy of CIK therapy. PLoS One 2013; 8: e69044.
[15] Gao Y, Zhao H, Ren M, Chen Q, Li J, Li Z, Yin C and Yue W. TOP2A promotes tumorigenesis of high-grade serous ovarian cancer by regulating the TGF-β/Smad pathway. J Cancer 2020; 11: 4181-4192.
[16] Xu C, Chen Y, Long F, Ye J, Li X, Huang Q, Yao D, Wang X, Zhao J, Meng W, Mo X, Lu R, Fan C and Zhang T. Prognostic value and biological function of LRRN4 in colorectal cancer. Cancer Cell Int 2022; 22: 158.
[17] Liu B, Zhang Y, Fan Y, Wang S, Li Z, Deng M, Li C, Wang J, Ma R, Wang X, Wang Y, Xu L, Hou K, Che X, Liu Y and Qu X. Leucine-rich repeat neuronal protein-1 suppresses apoptosis of gastric cancer cells through regulation of Fas/FasL. Cancer Sci 2019; 110: 2145-2155.
[18] Sahu RK, Ruhi S, Jeppu AK, Al-Goshae HA, Syed A, Nagdev S, Widyowati R, Ekasari W, Khan J, Bhattacharjee B, Goyal M, Bhattacharya S and Jangde RK. Malignant mesothelioma tumours: molecular pathogenesis, diagnosis, and therapies accompanying clinical studies. Front Oncol 2023; 13: 1204722.
[19] Li R, Fang J, Huo B, Su YS, Wang J, Liu LG, Hu M, Cheng C, Zheng P, Zhu XH, Jiang DS and Wei X. Leucine-rich repeat neuronal protein 4 (LRRN4) potentially functions in dilated cardiomyopathy. Int J Clin Exp Pathol 2017; 10: 9925-9933.
[20] Casingal CR, Kikkawa T, Inada H, Sasaki Y and Osumi N. Identification of FMRP target mRNAs in the developmental brain: FMRP might coordinate Ras/MAPK, Wnt/β-catenin, and mTOR signaling during corticogenesis. Mol Brain 2020; 13: 167.
[21] Fukamachi K, Matsuoka Y, Ohno H, Hamaguchi T and Tsuda H. Neuronal leucine-rich repeat protein-3 amplifies MAPK activation by epidermal growth factor through a carboxyl-terminal region containing endocytosis motifs. J Biol Chem 2002; 277: 43549-43552.
[22] Zenonos K and Kyprianou K. RAS signaling pathways, mutations and their role in colorectal cancer. World J Gastrointest Oncol 2013; 5: 97-101.
[23] Burotto M, Chiou VL, Lee JM and Kohn EC. The MAPK pathway across different malignancies: a new perspective. Cancer 2014; 120: 3446-3456.
[24] Nikolaidi A, Fountzilas E, Fostira F, Psyrri A, Gogas H and Papadimitriou C. Neoadjuvant treatment in ovarian cancer: new perspectives, new challenges. Front Oncol 2022; 12: 820128.
[25] Mesnage SJL, Auguste A, Genestie C, Dunant A, Pain E, Drusch F, Gouy S, Morice P, Bentivegna E, Lhomme C, Pautier P, Michels J, Le Formal A, Cheaib B, Adam J and Leary AF. Neoadjuvant chemotherapy (NACT) increases immune infiltration and programmed death-ligand 1 (PD-L1) expression in epithelial ovarian cancer (EOC). Ann Oncol 2017; 28: 651-657.
[26] Hunia J, Gawalski K, Szredzka A, Suskiewicz MJ and Nowis D. The potential of PARP inhibitors in targeted cancer therapy and immunotherapy. Front Mol Biosci 2022; 9: 1073797.